Hindawi
Advances in Civil Engineering
Volume 2019, Article ID 4680672, 11 pages
https://doi.org/10.1155/2019/4680672

Research Article

Seismic Strength and Stiffness for Recycled Aggregate Concrete-Filled Steel Tube Frame

Xianggang Zhang,[1,2] Jianhui Yang ,[1,2] Yaozong Zhang,[2] and Xiang Gao[2]

[1]*Henan Province Engineering Laboratory of Eco-Architecture and the Built Environment, Henan Polytechnic University, Jiaozuo 454000, China*
[2]*School of Civil Engineering, Henan Polytechnic University, Jiaozuo 454000, China*

Correspondence should be addressed to Jianhui Yang; yangjianhui@hpu.edu.cn

Received 27 December 2018; Accepted 14 April 2019; Published 9 May 2019

Academic Editor: Giovanni Minafò

To study the seismic strength and stiffness for recycled aggregate concrete-filled steel tube (RACFST) frame, two-frame specimens made up of RACFST column and reinforced recycled aggregate concrete (RAC) beam were used for a seismic test under reversed low-cycle loading. The failure mechanism, hysteresis curve, strength attenuation, and stiffness degradation were determined for the specimens. The design methods for the story shear bearing capacity and stiffness for the single-layer single-span RACFST frame were discussed. It is shown that the seismic design requirements including "strong column weak beam" and "strong shear weak bending" can be met. The hysteresis curves are symmetric and the strength attenuation and rigidity degeneration change significantly, then change a little, and then significantly again under the same displacement. It is possible that the methods including elastic bending moment at the column end, plastic hinge at the column end, and plastic hinge at the column bottom can all be applied to the design calculation of the story shear bearing capacity for the single-layer single-span RACFST frame. The method adopted in this paper can be used to estimate the original elastic layer stiffness of the RACFST frame.

1. Introduction

The booming construction industry causes a large amount of construction waste from different sources [1–3]. According to related statistics from 1985 to 2013 [4] construction waste production increased at an average annual rate of 12.26% in China. Until 2013, the accumulated construction waste production exceeded 10 billion tons over the years without considering resource utilization. About 10,000 tons of construction waste occupies about 1 acre of landfill land, which not only greatly reduces the utilization efficiency of land resources, but also damages the local natural environment and seriously affects the living standards of urban residents [5–7]. Therefore, how to deal with construction waste scientifically and rationally becomes an urgent problem to be solved in the field of concrete research and application [8–10].

Recently, recycled aggregate concrete (RAC) technology has become an effective way to utilize construction waste resources [11, 12]. By the so-called RAC technology [13–15], the construction waste can be recycled, crushed, washed, and graded and then mixed to form recycled aggregates with a certain proportion and grading. After that, the recycled aggregates are used to replace partially or completely natural aggregates, such as sand and gravel. Finally, a mixture of cement and water is added to prepare a new concrete named RAC. The RAC technology can solve the problem of pollution and resource utilization of construction waste and improve the environment. It has been considered a green concrete technology for achieving sustainable development of building resources [16–18].

However, most of the recycled coarse aggregate in RAC comes from old buildings that have been demolished [19, 20]. Due to the early construction of such buildings, the strength grade of the concrete is low. During the crushing process, a large number of microcracks or cracks appearing inside the recycled aggregate will cause initial internal damage, while the surface of the recycled coarse aggregate is heavily attached. The hardened cement mortar makes the surface rough, and the number of needle-like particles is

high. Accordingly, the concrete prepared from the recycled aggregate has a lower strength and elastic modulus, according to published research reports. The results show that RAC can basically meet the requirements for ordinary concrete [2, 21, 22]. However, RAC is generally only used in non-load-bearing structures because of the difficulty and high cost of preparing high-strength and elastic modulus RAC. This fatal flaw seriously restricts further application and development of RAC structures.

To improve the mechanical properties of RAC and produce a green RAC, it is an effective way to impose exterior constraint on interior concrete [23, 24], the exterior constraint jacket can be steel tube, plastic tube, FRP, etc. Konno et al. [25] first proposed the structure of recycled aggregate concrete-filled steel tube (RACFST). The research shows that the RACFST structure can not only inherit the advantages of a high bearing capacity present in ordinary concrete-filled steel tube (CFST) structures, but also solve the problem of efficient utilization of construction waste.

The RACFST structure will be feasible [26, 27], for example, in high-rise and super-tall buildings in the seismic fortification area, on the treatment of postearthquake construction waste and the reconstruction of buildings. Therefore, it is necessary to conduct in-depth systematic research on the seismic performance of the RACFST structure. At present, scholars have carried out quasistatic studies for about 100 RACFST middle-long column specimens that mainly present the following characteristics:

(1) They have distinguished loading devices. The RACFST specimen loading model mainly includes three types: cantilever column type [28–31], hinged type at two ends [32, 33], and fixed type at two ends [34]. Most of them are cantilever column type and hinged loading models at both ends.

(2) They resembled research conclusions. The failure modes of the RACFST specimens are similar to that of CFST specimens [30, 31, 34]. With the increase of the replacement rate, the seismic performance indexes of RACFST specimens tend to decrease a little bit, such as hysteresis curve, strength, stiffness, ductility, and energy consumption [30, 31, 33, 34].

(3) On the finite element analysis of the RACFST column [35, 36], the constitutive model of the RAC used was only a uniaxial stress-strain relationship, and the effect of the replacement rate of the recycled aggregate was not fully considered.

To summarize, the mechanical properties of RACFST components are generally similar to those of ordinary CFST. Therefore, filling RAC inside a steel tube is an effective way to recycle construction waste.

As a type of steel and concrete composite structure with good application prospects, it is urgent to carry out in-depth research on the seismic performance at the structural level of RACFST and to explore its design calculation theory. At present, no reports on the seismic performance of the RACFST framework have been made. To this end, this paper conducts experimental research and theoretical analysis on the seismic performance, especially regarding the strength and stiffness of the RACFST frame. It also provides reference for the seismic design and application of the RACFST structure.

2. Test Overview

2.1. Test Specimen Design. The RAC used in the test had a strength grade of C40, the replacement ratio of the recycled coarse aggregate was 100%, and the ratio of 1 m^3 RAC was present as follows. The cement: sand: recycled coarse aggregate: water ratios equaled 435.7 : 564.3 : 1115.2 : 204.8. The recycled coarse aggregate had a particle size range of 5–20 mm and an apparent density and water absorption of 2655 kg/m^3 and 3.16%, respectively.

The elevation of the RACFST frame specimen is shown in Figure 1. The dimensions are in mm, D represents the outer diameter of the circular steel tube, and B represents the outer length of the square steel tube. In the circular frame specimens, the longitudinal reinforcement ratio in the volume for the reinforced RAC beam was 2.50%, the hooping ratio in the encrypted and nonencrypted zones was 0.57% and 0.38%, respectively. In the square frame specimens, the longitudinal reinforcement ratio in the volume for the reinforced RAC beam was 1.73%, the hooping ratio in encrypted and nonencrypted zones was 0.75% and 0.38%, respectively. The 8 mm thick cover plate was welded to the top of the steel tube, and the 100 mm high RACFST column was reserved for effective transmission of the axial load. The specific design parameters of the test specimens are shown in Table 1. The steel tube grade was Q235. At the end of loading, the vertical force of the RACFST column was mostly borne by the core RAC. In order to reflect the force transmission path and stress state of the RACFST column, the selected axial compression ratio was only related to the RAC. That is, the axial compression ratio was $n = N/f_cA_c$, where N was the axial load applied during the test, f_c was the measured RAC axial compressive strength, and n was 0.8.

2.2. Loading Device. The loading device is shown in Figure 2. First, the two 1500 kN hydraulic jacks were simultaneously applied to the same design vertical load at the top of the column. Then, the horizontal load was controlled by force and displacement. Before the specimen yielded, the load was controlled and graded, and the load was cycled once. After the specimen yielded, the displacement control was adopted, and the multiple of the yield displacement, Δ_y, was controlled by the step difference. Each stage of the displacement was cycled three times until the load dropped below 80% of the peak load. The test was then stopped.

3. Test Results and Discussion

3.1. Failure Mechanism. The failure modes for specimens KJ-1 and KJ-2 are shown in Figure 3. A curved crack appeared first at KJ-1 beam end and then gradually developed into a critical oblique crack at 1/7-1/6 of the beam span. Finally, the protective layer of RAC at the shear zone

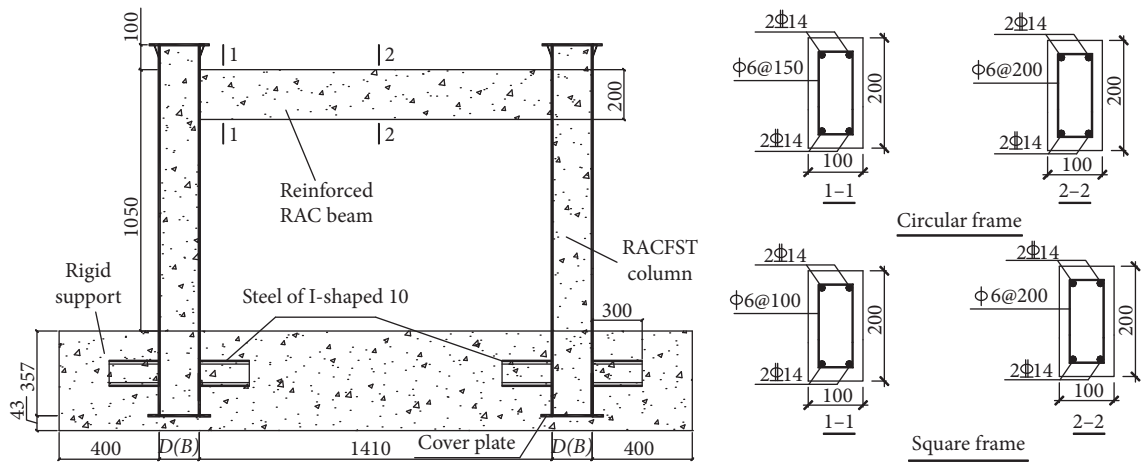

Figure 1: Elevation of the specimens.

Table 1: Specific design parameters of the specimens.

Number	Section form of steel tube	RACFST column (mm)		Reinforced RAC beam (mm)				Steel rate	Hoop coefficient of frame column
		Section size	Column height	Section size	Beam span	Measured diameter of longitudinal reinforcement	Measured diameter of stirrup		
KJ-1	Circular form	Φ166.2 × 4.6	950	100 × 200	1576.2	12.63	6.00	0.12	1.36
KJ-2	Square form	Φ150.9 × 5.0	950	100 × 200	1576.2	10.50	6.00	0.15	1.62

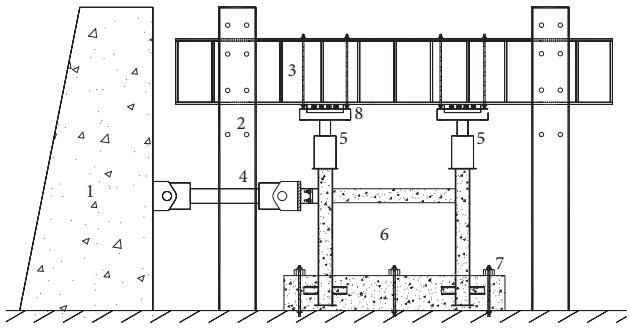

Figure 2: Loading device areas. 1: reaction wall of reinforced concrete; 2: steel column of vertical reaction; 3: reaction steel beam, connected with reaction steel column by high-strength bolt; 4: electrohydraulic servo actuator; 5: hydraulic jacks; 6: specimen; 7: pressure beam of steel structure; 8: roller device.

lifted up, forming a more obvious bending-shearing plasticity hinge. The bottom steel tube for specimen KJ-1 reached the yield strain and elastic-plastic buckling occurred due to bending. The curved cracks became the main part at the beam end for specimen KJ-2, and a curved plastic hinge was formed at last. In addition, the steel tube at the column bottom of specimen KJ-2 showed horizontal buckling. The hinge appeared first in the beam and then appeared in the column. This occurred for specimens KJ-1 and KJ-2 and indicated that the failure mechanism for the RACFST frame specimen belonged to the beam hinge one, which could meet the seismic design requirements for a "strong column weak beam" application. The order of the hinges for specimens KJ-1 and KJ-2 is shown in Figures 4 and 5.

The bending-shearing failure occurred at the beam end of the specimen KJ-1, and the bending failure occurred at the beam end of the specimen KJ-2. All met the seismic design requirements for a "strong shear weak bending" application.

3.2. Hysteresis Curve of Load versus Vertex Displacement. The hysteresis curves for the load versus vertex displacement for the specimens are shown in Figure 6, where P represents the load and Δ represents the displacement. It can be seen that the hysteresis curves for specimens KJ-1 and KJ-2 are basically symmetrical and have good stability. During the whole test process, the hysteresis curve was not pinched. This was mainly due to the lateral restraint of the outer steel tube to the core RAC, which improved the strength and deformation performance of the core RAC. Thus, a sudden change in the lateral stiffness of the frame specimens cannot happen. In general, the hysteresis curves show a relatively full shuttle shape, and the energy consumption of the specimens was good.

3.3. Strength Attenuation. The strength attenuation for specimens KJ-1 and KJ-2 under the same cyclic displacement is shown in Figure 7, where Δ_y refers to the yield displacement and P_i represents the control displacement load of the ith cycle under a certain control displacement. The values of i are 1, 2, and 3. The parameter P_{j1} refers to the control displacement load of the first cycle under the jth cyclic displacement. The values of j are 1, 2, 3, 4, and even higher if possible. It can be seen that the strength attenuation

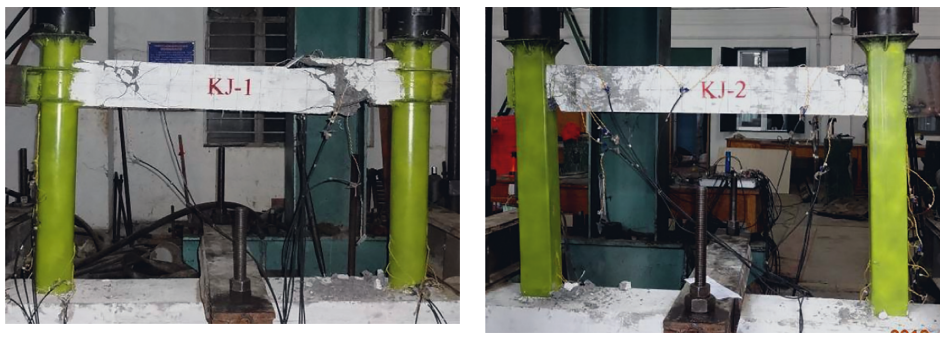

(a) (b)

Figure 3: Overall failure mode: (a) specimen KJ-1, (b) specimen KJ-2.

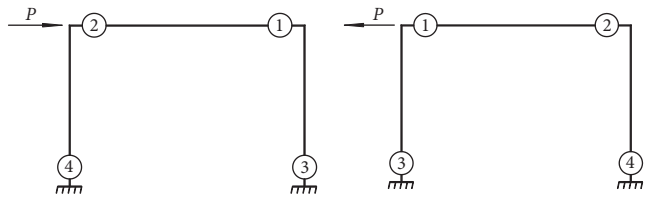

(a) (b)

Figure 4: The order of KJ-1 plastic hinge formation: (a) right horizontal load, (b) left horizontal load.

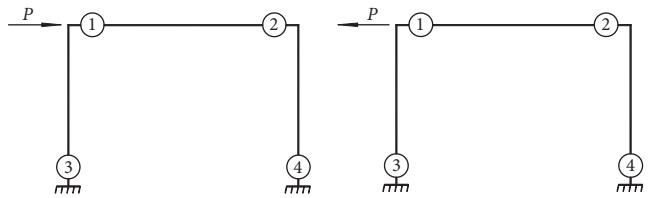

(a) (b)

Figure 5: The order of KJ-2 plastic hinge formation: (a) right horizontal load, (b) left horizontal load.

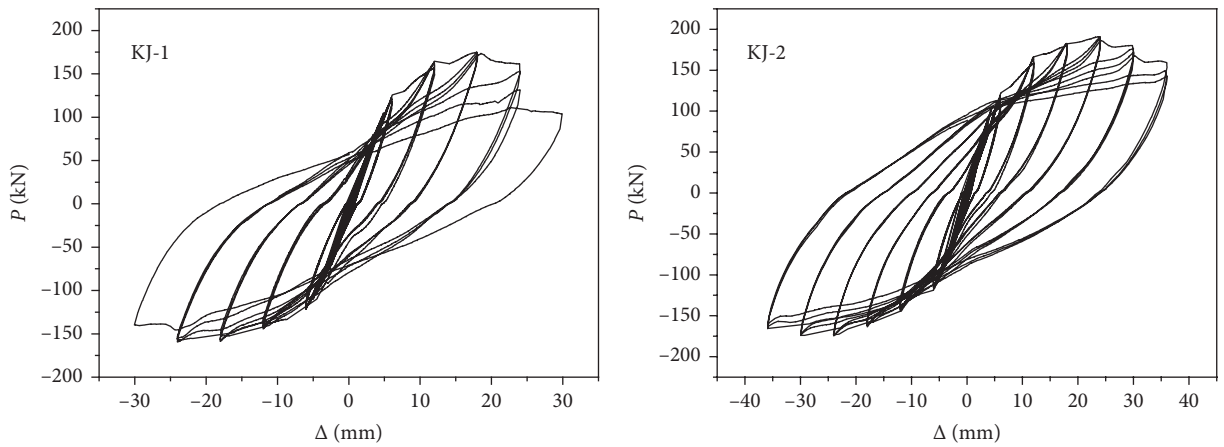

(a) (b)

Figure 6: Hysteresis curves for specimens: (a) specimen KJ-1, (b) specimen KJ-2.

went from a larger to a smaller and then to a larger process. At the initial stage of the displacement control, there were more bending cracks at the beam end, and the bearing capacity showed a large attenuation for the first time. At this stage, the maximum strength attenuation for specimens KJ-1 and KJ-2 was 0.967 and 0.950, respectively. As the loading

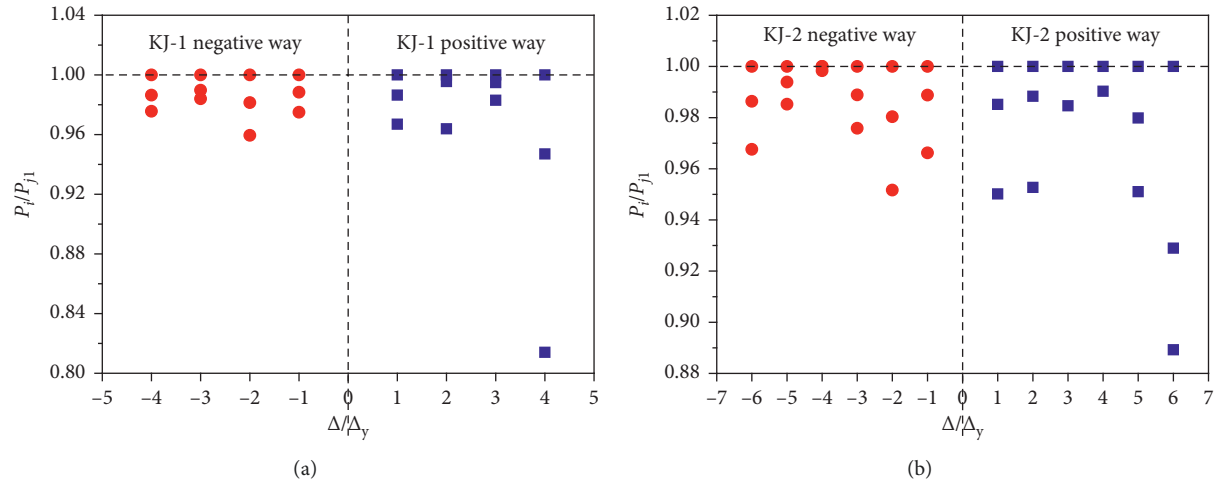

Figure 7: Strength attenuation of specimens: (a) specimen KJ-1, (b) specimen KJ-2.

continued, the crack was restrained by the longitudinal reinforcement and stirrups inside the beam. New cracks no longer appeared, the cracks at the beam ends were basically complete, and the old cracks did not extend and just widened slightly. At this moment, the bearing capacity of the reinforced RAC beam reduced slightly, and the strength attenuation for the specimens KJ-1 and KJ-2 was the smallest. Specifically, when the cyclic displacement reached ±3Δ and ±4Δ, the minimum strength attenuation for specimens KJ-1 and KJ-2 was 0.983 and 0.990, respectively. With the appearance and development of the plastic hinge at the column end, the strength attenuation increased again. At the end of loading, the strength attenuation reached the maximum, and the specimens KJ-1 and KJ-2 had values 0.814 and 0.889, respectively.

3.4. Stiffness Degradation. The stiffness degradation for specimens KJ-1 and KJ-2 under the same cyclic displacement is shown in Figure 8, where K_i refers to the secant stiffness of each cycle under the same cyclic displacement; i is 1, 2, and 3; and K_{j1} refers to the secant stiffness of the first cycle under each cyclic displacement. It can be seen that the stiffness degradation for specimens KJ-1 and KJ-2 was larger and then smaller and then larger again, similar to the law of strength attenuation. When the stiffness had a large attenuation at first, the maximum stiffness degradation for specimens KJ-1 and KJ-2 reached 0.970 and 0.954, respectively. When the cyclic displacement reached ±3Δ and ±4Δ, the minimum stiffness degradation for specimens KJ-1 and KJ-2 reached 0.989 and 0.994, respectively. When the stiffness showed again a large attenuation, the maximum stiffness degradation for specimens KJ-1 and KJ-2 reached 0.896 and 0.920, respectively.

The stiffness degradation for specimens KJ-1 and KJ-2 under each cyclic displacement is shown in Figure 9. It can be seen that as the cyclic displacement increased, the secant stiffness gradually decreased, and the stiffness deterioration went from fast to slow throughout the whole test. This is mainly because the new cracks appeared before the specimens yielded fully, and the growth rate of the bearing capacity was smaller than the growth rate of the displacement. Thus, the stiffness degradation was rapid. After the peak load, with the development of the plastic hinge at the beam end and the appearance of the plasticity hinge at the column end, the good deformation ability made the bearing capacity decrease slowly. At this time, the decrease rate of the bearing capacity was less than the growth rate of the displacement, and the stiffness degradation was slow.

4. Strength Calculation

In the elastic-plastic seismic response calculation and seismic identification of the frame, the story shear bearing capacity is an important control parameter. The results show that it is simple and easy to calculate the shear bearing capacity for reinforced concrete structure under the multilayer multispan by the plastic hinge at the column bottom method [37]. Moreover, the calculation results were more moderate and practical. The single-layer single-span frame designed in this paper belongs to a special frame form. Based on the method of elastic bending moment at the column end, the plastic hinge at the column end, and plastic hinge at the column bottom, it is possible to discuss the calculation method for the strength of a single-layer single-span frame of RACFST.

The beam hinge failure occurred in the RACFST frame specimen as shown in the experimental results. This could be seemed as a type of nonstrong beam and nonweak column, and the RACFST column was broken due to bending. The abovementioned result is the applicable premise for the three calculation methods. The shear bearing capacity of the frame is composed of the shear bearing capacity of each column. When the failure modes of the columns are the same, the story shear bearing capacity is approximately equal to the sum of the shear bearing capacity of each column.

In the absence of experimental verification, whether the frame belongs to the type of nonstrong beam and

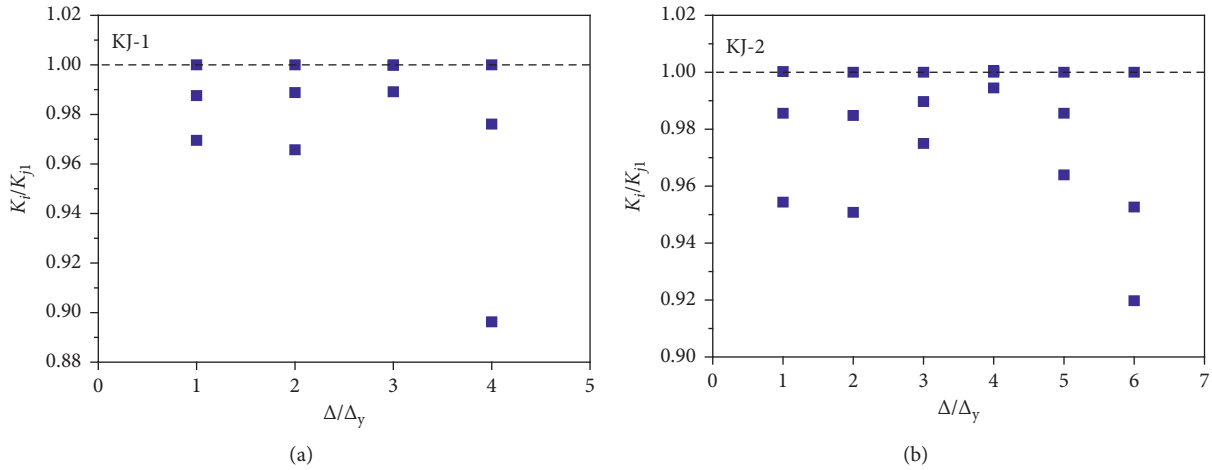

Figure 8: Stiffness degradation of specimen under the same cyclic displacement: (a) specimen KJ-1; (b) specimen KJ-2.

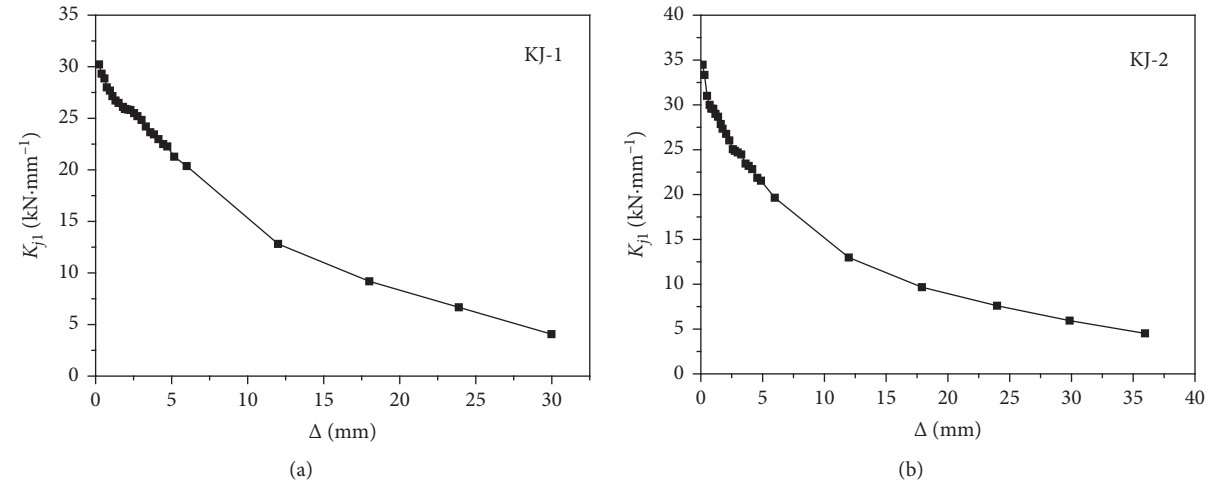

Figure 9: Stiffness degradation of specimens under each cyclic displacement: (a) specimen KJ-1, (b) specimen KJ-2.

nonweak column, or not, needs to be determined by the yield bending moment at the node position. When $\sum M_{yc} > \sum M_{yb}$, the node is a weak beam type, and the strong beam type appears in the opposite case. Among them, $\sum M_{yb}$ and $\sum M_{yc}$ are the sum of the actual yield bending moments of the beam end and the column end at the same node, respectively. The actual yield bending moment is calculated based on the strength standard values of the actual reinforcement and material. In this paper, the steel tube and RAC used were taken as measured values. For the joint of a weak beam type, the beam end yields first, and the corresponding column end may be in an elastic state. Also, a plastic hinge may appear at the column bottom or at the column top. Correspondingly, the three calculation methods for the story shear bearing capacity are presented as follows.

4.1. Method for Elastic Bending Moment at the Column End. The basic principle is that the beam end yields first, and the corresponding column end is in an elastic working state. The elastic bending moment can be expressed by equations (1) and (2).

For the upper node of this layer column,

$$M_c^t = \sum M_{yb}^t \times \frac{i_c}{i_c + i_{c+1}}. \quad (1)$$

And for the lower node of this layer column,

$$M_c^b = \sum M_{yb}^b \times \frac{i_c}{i_c + i_{c-1}}, \quad (2)$$

where M_c^t and M_c^b are the elastic bending moments of the upper and lower column ends at this layer, respectively; $\sum M_{yb}^t$ and $\sum M_{yb}^b$ are the sum of the yield bending moments of the upper and lower ends of beam corresponding to the column at this layer, respectively; i_c, i_{c+1}, and i_{c-1} are the line stiffness of the columns at this layer and the adjacent upper and lower layers, respectively.

Therefore, three different cases of plastic hinges are obtained, so different calculation formulas can be employed, as shown in Figure 10.

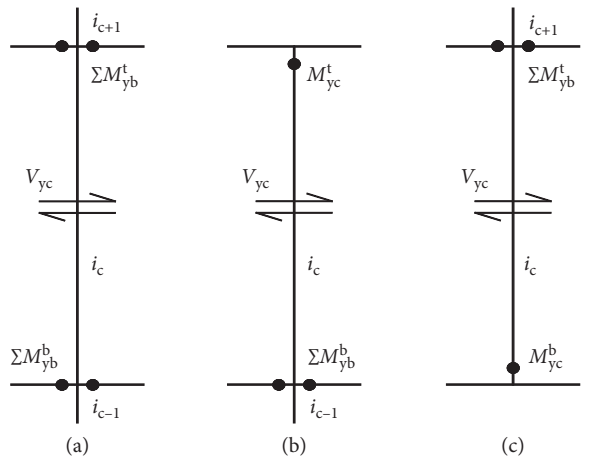

Figure 10: Method of elastic bending moment at the column end: (a) middle layer, (b) top layer, (c) bottom layer.

The equations for Figures 10(a)–10(c) are as follows:

$$V_{yc} = \frac{M^t_c + M^b_c}{h},$$
$$V_{yc} = \frac{M^t_{yc} + M^b_c}{h}, \quad (3)$$
$$V_{yc} = \frac{M^t_c + M^b_{yc}}{h},$$

where h is the net height of the column.

The shear bearing capacity for two-frame specimens of single-layer single-span designed in this paper should be calculated according to Figure 10(c) and $i_{c+1} = 0$.

4.2. Method for Plastic Hinge at the Column End. The basic principle is that under earthquake effect, if the plastic hinge appears first at the beam end, then when the earthquake effect continues to increase, the bending moment of the column end continues to grow until the upper or lower ends of the node reach the yield bending moment. This means that the plasticity hinge occurs. Therefore, when this method is adopted, the node of the weak beam type is first confirmed, and then it is necessary to determine that a certain column end of the node yields first.

First, the node of weak beam type is confirmed as follows:

$$\sum M^t_{yb} \times \frac{i_c}{i_c + i_{c+1}} < M^t_{yc}, \quad (4)$$

$$\sum M^t_{yb} \times \frac{i_{c+1}}{i_c + i_{c+1}} < M^{b'}_{yc}, \quad (5)$$

where $M^{b'}_{yc}$ is the yield bending moment of the column bottom section at the upper layer. The node suitable for equation (4) or equation (5) is a node of weak beam type.

At the upper node of this layer column, if

$$M^{b'}_{yc} \times \frac{i_c}{i_{c+1}} < M^t_{yc}, \quad (6)$$

then the plastic hinge first appears at the column bottom at the upper layer. In the opposite case, the plastic hinge first appeared at the column top at this layer.

At the lower node of this layer column, if

$$M^{t'}_{yc} \times \frac{i_c}{i_{c-1}} < M^b_{yc}, \quad (7)$$

where $M^{t'}_{yc}$ is the yield bending moment of the column top section at the lower layer. Then, the plastic hinge first appears on the column top at the lower layer. In the opposite case, the plastic hinge appears first on the column bottom at this layer.

Therefore, three different cases of plastic hinges are obtained, so different calculation formulas are employed, as shown in Figure 11.

The calculation formulas for Figures 11(a)–11(c) are as follows:

$$V_{yc} = \frac{M^t_{yc} + M^{t'}_{yc} \times i_c/i_{c-1}}{h},$$
$$V_{yc} = \frac{M^b_{yc} + M^{b'}_{yc} \times i_c/i_{c+1}}{h}, \quad (8)$$
$$V_{yc} = \frac{M^{b'}_{yc} \times i_c/i_{c+1} + M^{t'}_{yc} \times i_c/i_{c-1}}{h}.$$

The story shear bearing capacity for two-frame specimens of single-layer single-span designed in this paper should be calculated according to Figure 11(b) and $i_{c+1} = 0$. According to the principle of node balance, $M^{b'}_{yc} \times i_c/i_{c+1} = \sum M^t_{yb}$.

4.3. Method for Plastic Hinge at the Column Bottom. The basic principle is that after the plastic hinge appears at the beam end, the plastic hinge always appears at the bottom of the corresponding column. When the beam end yields, the bending moment of column top at this layer can be approximately calculated by

$$M^t_c = \sum M^t_{yb} \times \frac{i_c}{i_c + i_{c+1}}. \quad (9)$$

Therefore, three different cases of plastic hinges are obtained, so different calculation formulas are employed, as shown in Figure 12.

The calculation formulas for Figures 12(a)–12(c) are as follows:

$$V_{yc} = \frac{M^t_{yc} + M^b_{yc}}{h},$$
$$V_{yc} = \frac{M^t_c + M^b_{yc}}{h}, \quad (10)$$
$$V_{yc} = \frac{M^t_c + M^b_{yc}}{h}.$$

The story shear bearing capacity for two-frame specimens of single-layer single-span designed in this paper should be calculated according to Figure 12(b) and $i_{c+1} = 0$.

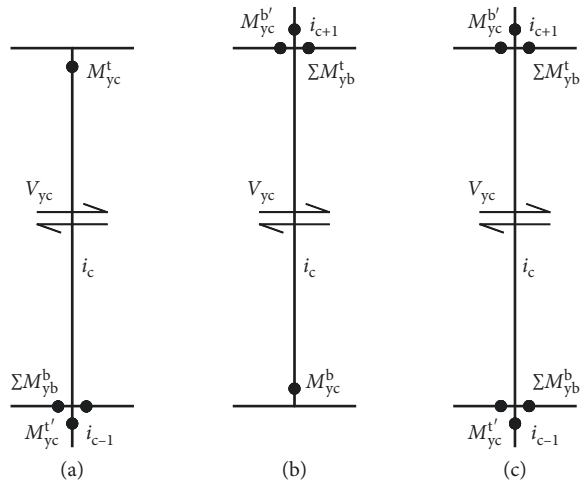

Figure 11: Method of plastic hinge at the column end: (a) top layer, (b) bottom layer, and (c) middle layer.

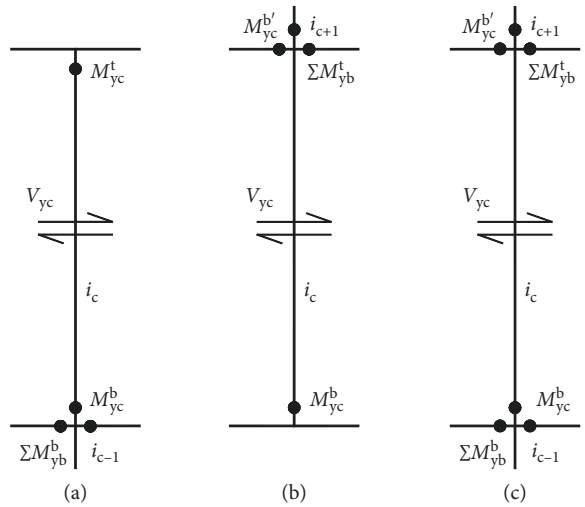

Figure 12: Method of plastic hinge at the column bottom: (a) top layer, (b) bottom layer, and (c) middle layer.

After the shear bearing capacity of the frame column is determined, the story shear bearing capacity of the frame specimens can be calculated as follows:

$$V_y = \sum V_{yc}. \tag{11}$$

According to the preliminary research results [38, 39], the bending bearing capacity for a normal section of the RAC-filled circular steel tube column can be designed and calculated by the specification DL/T 5085-1999. The normal section bending bearing capacity of the RAC-filled square steel tube column can be calculated by the specification GJB 4142-2000, where a reduction factor of 0.92 needed to be multiplied. The specification DBJ 13-51-2010 can also be used, where an amplification factor of 1.13 is needed.

The actual bending bearing capacity, M_{yb}, for a normal section for the reinforced RAC beam can be calculated as follows:

$$M_{yc} = f_y A_s (h_0 - \alpha_s'), \tag{12}$$

where f_y is the measured yield strength of the reinforcement, A_s is the total cross-sectional area of the longitudinal reinforcement in tension, h_0 is the effective height of the cross section, and α_s' is the distance from the action point of all the longitudinal reinforcement in tension to the compressive edge of the cross section.

The story shear bearing capacity of the frame specimens was calculated by the above three methods. The calculated values and test values are shown in Table 2.

It can be seen in Table 2 that the designed nodes in this paper are of the weak beam type based on the criteria. The test values for the story shear bearing capacity for RACFST frame specimens were in good agreement with the calculated values, and the calculated values obtained by the three calculation methods were consistent. This is because for the single-layer single-span frame, all three calculation methods showed after the plastic hinge of the beam ends appeared, the hinges in a plastic state occurred at the column bottom, while the column top remained an elastic working state. Although the equations for the three methods were not consistent, the results were essentially the same. In other words, the story shear bearing capacity for the single-layer single-span RACFST frame can be calculated by the method for elastic bending moment at the column end, the method for plastic hinge at the column end, or the method for plastic hinge at the column bottom.

5. Stiffness Calculation

Under the horizontal load, the calculation method for the initial elastic layer stiffness for the RACFST frame [40] is as follows:

$$S = S' - \beta\left(\frac{k}{\pi}\right)^2 \frac{P}{h}, \tag{13}$$

$$S' = \frac{\beta i_c}{h^2}, \tag{14}$$

$$\beta = \frac{12(r_1 r_2 + r_1 + r_2)}{r_1 r_2 + 4(r_1 + r_2) + 12}, \tag{15}$$

$$r_1 = \frac{6(i_1 + i_2)}{i_c + i_{c2}}, \tag{16}$$

$$r_2 = \frac{6(i_3 + i_4)}{i_c + i_{c2}}, \tag{17}$$

$$\tan\left(\frac{\pi}{k}\right) = \frac{(\pi/k)(r_1 + r_2)}{(\pi/k)^2 - r_1 r_2}, \tag{18}$$

where S is the lateral stiffness of the column under axial force, S' is the lateral stiffness of the column without axial force, and k is the calculation length coefficient of the unsupported column with the rotation restraint of the two ends. The solution for equation (18) is the value of k.

Table 2: Comparison between calculated values and test values of story shear bearing capacity for RACFST frames.

Number	$\sum M_{yc}$ (kN·mm)	$\sum M_{yb}$ (kN·mm)	Calculated value V_c (kN)			Test value V_t (kN)	V_c/V_t
			Method for elastic bending moment at the column end	Method for plastic hinge at the column end	Method for plastic hinge at the column bottom		
KJ-1	57.61	14.46	169.57	169.57	169.57	165.38	1.03
KJ-2	61.03	11.36	170.34	170.34	170.34	182.39	0.93

Also, P is the vertical load; h is the column height; i_1, i_2, i_3, and i_4 are the corresponding line stiffnesses of the beams; i_c, i_{c1}, and i_{c2} are the corresponding line stiffnesses of the columns; r_1 and r_2 represent the ratios of the couple moment of restraint to the line stiffness of column at the A and B ends, respectively. These parameters are shown in Figure 13.

For the two-frame specimens with a single-layer single-span design described in this paper, $i_1 = i_3 = 0$ or $i_2 = i_4 = 0$, and $i_{c1} = i_{c2} = 0$. Since the bottom end of the frame specimen is fixed, $r_2 = \infty$.

The bending stiffness, EI, for circular and square frame columns can be calculated by the standard DBJ 13-51-2010 and AIJ 1997, respectively. The calculation for DBJ 13-51-2010 is as follows:

$$EI = E_s I_s + \alpha E_c I_c, \tag{19}$$

where E_s and E_c are the elastic moduli of steel tube and concrete, respectively; and I_s and I_c are the inertia moment of steel tube and concrete, respectively. For the concrete-filled circular steel tube, $\alpha = 0.8$, and for concrete-filled square steel tube, $\alpha = 0.6$. The calculation for AIJ 1997 is as follows:

$$EI = E_s I_s + 0.2 E_c I_c. \tag{20}$$

The bending stiffness of the frame beam was calculated by the code for the concrete structure design (GB50010-2010). After the lateral stiffness of the RACFST column was determined, the lateral stiffness of the underlying columns was summed to obtain the initial elastic layer stiffness for the RACFST frame, as shown in Table 3.

As seen in Table 3, the calculated values for the lateral stiffness are generally in agreement with the test values. The above method can be used to estimate the initial elastic layer stiffness of the RACFST frame. It should be noted that the test-measured value of the initial elastic layer stiffness was taken as the ratio of the sum of the absolute values for the first-stage positive and negative loads to the sum of the absolute values for the corresponding deformation during the force-controlled loading. When the force control started, the load and displacement were relatively small at the beginning of the load control. Therefore, it was easy to have a large influence on the initial elastic layer stiffness so that the calculated value might deviate greatly from the test value.

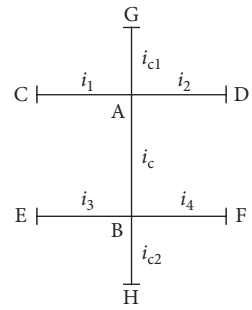

Figure 13: Beam and column with line stiffness.

Table 3: Calculated values and test values of initial elastic layer stiffness of RACFST specimens.

Number	Calculated S_c' (kN·mm^{-1})	Test value S_t' (kN·mm^{-1})	S_c'/S_t'
KJ-1	39.24	30.22	1.30
KJ-2	35.10	34.48	1.02

6. Conclusions

Under the reversed low-cycle loading, the experimental study of the strength and stiffness of the two-frame specimens made up of RACFST column and reinforced RAC beam indicates the following:

(1) The failure mechanism of the specimens KJ-1 and KJ-2 reaches the seismic design requirements for "strong column weak beam" and "strong shear weak bending." The hysteresis curves are basically symmetrical presenting good stability.

(2) The strength attenuation and stiffness degradation of the specimens KJ-1 and KJ-2 under the same cyclic displacement generally go from a larger to a smaller and then a larger again process. The stiffness degradation of the specimen under each cyclic displacement goes from fast to slow.

(3) It is shown that the method for elastic bending moment at the column end, the method for plastic hinge at the column end, and the method for plastic hinge at the column bottom can all be used to design the calculation for the story shear bearing capacity for the single-layer single-span RACFST frame.

(4) The method in this paper can be used to estimate the initial elastic layer stiffness of the RACFST frame.

Data Availability

The experimental data used to support the findings of this study are included within the article.

Conflicts of Interest

The authors declare that there are no conflicts of interest regarding the publication of this paper.

Acknowledgments

This research was financially supported by the Science and Technology Breakthrough Project of Henan Province (172102210285), the Fundamental Research Funds for the Universities of Henan Province (NSFRF170921), and the Safe Production Project of Key Technology for Major Accident Prevention and Control (Henan-0006-2016AQ). The authors are grateful to the authority for the support.

References

[1] J. Xiao, M. Tawana, and X. Huang, "Review of studies on structural performance of recycled aggregate concrete in China," *Science China Technological Sciences*, vol. 55, no. 10, pp. 2727–2739, 2012.

[2] M. Etxeberria, E. Vázquez, A. Marí, and M. Barra, "Influence of amount of recycled coarse aggregates and production process on properties of recycled aggregate concrete," *Cement and Concrete Research*, vol. 37, no. 5, pp. 735–742, 2007.

[3] K. McNeil and T. H. K. Kang, "Recycled concrete aggregates: a review," *International Journal of Concrete Structures and Materials*, vol. 7, no. 1, pp. 61–69, 2008.

[4] T. Ding, J. Xiao, V. W. Y. Tam, and W. Y. Vivian, "A closed-loop life cycle assessment of recycled aggregate concrete utilization in China," *Waste Management*, vol. 56, pp. 367–375, 2016.

[5] S. Marinkovic, V. Radonjanin, M. Malesev, and I. Ignjatovic, "Comparative environmental assessment of natural and recycled aggregate concrete," *Waste Management*, vol. 30, no. 11, pp. 2255–2264, 2010.

[6] R. V. Silva, J. de Brito, and R. K. Dhir, "Properties and composition of recycled aggregates from construction and demolition waste suitable for concrete production," *Construction and Building Materials*, vol. 65, pp. 201–217, 2014.

[7] T. Uygunoglu, I. B. Topcu, and A. G. Celik, "Use of waste marble and recycled aggregates in self-compacting concrete for environmental sustainability," *Journal of Cleaner Production*, vol. 84, pp. 691–700, 2014.

[8] S. Jayakody, A. M. Z. Zimar, and R. A. L. M. Ranaweera, "Potential use of recycled construction and demolition waste aggregates for non- structural concrete applications," *Journal of the National Science Foundation of Sri Lanka*, vol. 46, no. 2, pp. 205–216, 2018.

[9] P. S. Martinez, M. G. Cortina, F. F. Martinez, and A. R. Sanchez, "Comparative study of three types of fine recycled aggregates from construction and demolition waste (CDW) and their use in masonry mortar fabrication," *Journal of Cleaner Production*, vol. 118, pp. 162–169, 2016.

[10] D. Xuan, C. S. Poon, and W. Zheng, "Management and sustainable utilization of processing wastes from ready-mixed concrete plants in construction: a review," *Resources, Conservation and Recycling*, vol. 136, pp. 238–247, 2018.

[11] M. Behera, S. K. Bhattacharyya, A. K. Minocha, R. Deoliya, and S. Maiti, "Recycled aggregate from C&D waste & its use in concrete-a breakthrough towards sustainability in construction sector: a review," *Construction and Building Materials*, vol. 68, pp. 501–516, 2014.

[12] V. W. Y. Tam and C. M. Tam, "A review on the viable technology for construction waste recycling," *Resources, Conservation and Recycling*, vol. 47, no. 3, pp. 209–221, 2006.

[13] Z. H. Duan and C. S. Poon, "Properties of recycled aggregate concrete made with recycled aggregates with different amounts of old adhered mortars," *Materials & Design*, vol. 58, pp. 19–29, 2014.

[14] S. R. riravindrarajah, N. D. H. Wang, and L. J. W. Ervin, "Mix design for pervious recycled aggregate concrete," *International Journal of Concrete Structures and Materials*, vol. 6, no. 4, pp. 239–246, 2012.

[15] L. Evangelista and J. de Brito, "Concrete with fine recycled aggregates: a review," *European Journal of Environmental and Civil Engineering*, vol. 18, no. 2, pp. 129–172, 2014.

[16] D. Xuan, B. Zhan, and C. S. Poon, "Assessment of mechanical properties of concrete incorporating carbonated recycled concrete aggregates," *Cement and Concrete Composites*, vol. 65, pp. 67–74, 2016.

[17] J. K. Zhang, C. J. Shi, Y. K. Li, X. Y. Pan, C. S. Poon, and Z. B. Xie, "Performance enhancement of recycled concrete aggregates through carbonation," *Journal of Materials in Civil Engineering*, vol. 27, no. 11, article 04015029, 2015.

[18] P. Belin, G. Habert, M. Thiery, and N. Roussel, "Cement paste content and water absorption of recycled concrete coarse aggregates," *Materials and Structures*, vol. 47, no. 9, pp. 1451–1465, 2014.

[19] E. Anastasiou, K. Georgiadis Filikas, and M. Stefanidou, "Utilization of fine recycled aggregates in concrete with fly ash and steel slag," *Construction and Building Materials*, vol. 50, pp. 154–161, 2014.

[20] M. Pepe, R. D. Toledo Filho, E. A. B. Koenders, and E. Martinelli, "Alternative processing procedures for recycled aggregates in structural concrete," *Construction and Building Materials*, vol. 69, pp. 124–132, 2014.

[21] K. P. Verian, W. Ashraf, and Y. Z. Cao, "Properties of recycled concrete aggregate and their influence in new concrete production," *Resources Conservation and Recycling*, vol. 133, pp. 30–49, 2016.

[22] C. Barra, Y. Li, J. Zhang, W. Li, L. Chong, and Z. Xie, "Performance enhancement of recycled concrete aggregate-a review," *Journal of Cleaner Production*, vol. 112, pp. 466–472, 2016.

[23] A. Cascardi, F. Micelli, and M. A. Aiello, "An artificial neural networks model for the prediction of the compressive strength of FRP-confined concrete circular columns," *Engineering Structures*, vol. 140, pp. 199–208, 2017.

[24] G. Amato, G. Campione, L. Cavaleri, G. Minafò, and N. Miraglia, "The use of pumice lightweight concrete for masonry applications," *Materials and structures*, vol. 45, no. 5, pp. 679–693, 2012.

[25] K. Konno, Y. Sato, and Y. Kakuta, "Property of recycled concrete column encased by steel tube subjected to axial compression," *Transactions of the Japan Concrete Institute*, vol. 19, no. 2, pp. 231–238, 1997.

[26] Z. Chen, J. Xu, Y. Chen, and E. M. Lui, "Recycling and reuse of construction and demolition waste in concrete-filled steel tubes: a review," *Construction and Building Materials*, vol. 126, pp. 641–660, 2016.

[27] J. Xiao, Y. Huang, and Z. Sun, "Seismic behavior of recycled aggregate concrete filled steel and glass fiber reinforced plastic tube columns," *Advances in Structural Engineering*, vol. 17, no. 5, pp. 693–707, 2014.

[28] B. Wu, X.-Y. Zhao, and J.-S. Zhang, "Cyclic behavior of thin-walled square steel tubular columns filled with demolished

concrete lumps and fresh concrete," *Journal of Constructional Steel Research*, vol. 77, pp. 69–81, 2012.

[29] Y. Huang, J. Xiao, and L. Shen, "Damage assessment for seismic response of recycled concrete filled steel tube columns," *Earthquake Engineering and Engineering Vibration*, vol. 15, no. 3, pp. 607–616, 2016.

[30] Y.-C. Tang, L.-J. Li, W.-X. Feng, F. Liu, and B. Liao, "Seismic performance of recycled aggregate concrete-filled steel tube columns," *Journal of Constructional Steel Research*, vol. 133, pp. 112–124, 2017.

[31] Z. Chen, C. Jing, J. Xu, and X. Zhang, "Seismic performance of recycled concrete-filled square steel tube columns," *Earthquake Engineering and Engineering Vibration*, vol. 16, no. 1, pp. 119–130, 2017.

[32] Y.-F. Yang, L.-H. Han, and L.-T. Zhu, "Experimental Performance of recycled aggregate concrete-filled circular steel tubular columns subjected to cyclic flexural loadings," *Advances in Structural Engineering*, vol. 12, no. 2, pp. 183–194, 2009.

[33] Y.-F. Yang and L.-T. Zhu, "Recycled aggregate concrete filled steel SHS beam-columns subjected to cyclic loading," *Steel & Composite structures*, vol. 9, no. 1, pp. 19–38, 2009.

[34] W. Q. Li, X. X. Zha, and M. Yu, "Seismic behavior study of hollow ordinary concrete and recycled aggregate concrete filled steel tubular (CFST) columns I: experimental and FEM study," *Progress in Steel Building Structures*, vol. 14, no. 3, pp. 27–35, 2014, in Chinese.

[35] J.-J. Xu, Z.-P. Chen, J.-Y. Xue, Y.-L. Chen, and J.-T. Zhang, "Simulation of seismic behavior of square recycled aggregate concrete-filled steel tubular columns," *Construction and Building Materials*, vol. 149, pp. 553–566, 2017.

[36] Y.-F. Yang, "Modelling of recycled aggregate concrete-filled steel tube (RACFST) beam-columns subjected to cyclic loading," *Steel and Composite Structures*, vol. 18, no. 1, pp. 213–233, 2015.

[37] L. Wei and D. H. Li, "Calculation method of yielding shear strength for reinforced concrete frame layer," *Building Structure*, vol. 17, no. 6, pp. 1–6, 1987, in Chinese.

[38] X. G. Zhang, Z. P. Chen, J. Y. Xue, and Y. S. Su, "Experimental study on seismic behavior of recycled aggregate concrete filled steel tube columns," *China Civil Engineering Journal*, vol. 47, no. 9, pp. 45–56, 2014, in Chinese.

[39] X. G. Zhang, Z. P. Chen, J. Y. Xue, and Y. S. Su, "Experimental study on seismic behavior of recycled aggregate concrete filled square steel tube columns," *Journal of Building Structures*, vol. 35, no. 9, pp. 11–19, 2014, in Chinese.

[40] Q. Z. Li and P. Liang, "Lateral stiffnesses of columns in frame," *Journal of South China University of Technology*, vol. 23, no. 1, pp. 91–99, 1995, in Chinese.